



**HAL**  
open science

## FUNCTIONAL AND STRUCTURAL ANALYSIS OF FIVE MUTATIONS IDENTIFIED IN METHYLMALONIC ACIDURIA *cbIB* TYPE

Ana Jorge-Finnigan, Cristina Aguado, Rocio Sanchez-Alcudia, David Abia,  
Eva Richard, Begoña Merinero, Alejandra Gámez, Ruma Banerjee, Lourdes R  
Desviat, Magdalena Ugarte, et al.

► **To cite this version:**

Ana Jorge-Finnigan, Cristina Aguado, Rocio Sanchez-Alcudia, David Abia, Eva Richard, et al.. FUNCTIONAL AND STRUCTURAL ANALYSIS OF FIVE MUTATIONS IDENTIFIED IN METHYLMALONIC ACIDURIA *cbIB* TYPE. *Human Mutation*, 2010, 31 (9), pp.1033. 10.1002/humu.21307 . hal-00555317

**HAL Id: hal-00555317**

**<https://hal.science/hal-00555317>**

Submitted on 13 Jan 2011

**HAL** is a multi-disciplinary open access archive for the deposit and dissemination of scientific research documents, whether they are published or not. The documents may come from teaching and research institutions in France or abroad, or from public or private research centers.

L'archive ouverte pluridisciplinaire **HAL**, est destinée au dépôt et à la diffusion de documents scientifiques de niveau recherche, publiés ou non, émanant des établissements d'enseignement et de recherche français ou étrangers, des laboratoires publics ou privés.



**FUNCTIONAL AND STRUCTURAL ANALYSIS OF FIVE  
MUTATIONS IDENTIFIED IN METHYLMALONIC ACIDURIA  
cbIB TYPE**

Journal:	<i>Human Mutation</i>
Manuscript ID:	humu-2009-0515.R2
Wiley - Manuscript type:	Research Article
Date Submitted by the Author:	14-May-2010
Complete List of Authors:	Jorge-Finnigan, Ana; Centro de Diagnóstico de Enfermedades Moleculares. Centro de Biología Molecular Aguado, Cristina; Centro de Diagnóstico de Enfermedades Moleculares. Centro de Biología Molecular Sanchez-Alcudia, Rocio; Centro de Diagnóstico de Enfermedades Moleculares. Centro de Biología Molecular Abia, David; Servicio de Bioinformática, Centro de Biología Molecular Richard, Eva; Centro de Diagnóstico de Enfermedades Moleculares. Centro de Biología Molecular Merinero, Begoña; Centro de Diagnóstico de Enfermedades Moleculares. Centro de Biología Molecular Gámez, Alejandra; Centro de Diagnóstico de Enfermedades Moleculares., Centro de Biología Molecular Banerjee, Ruma; University of Michigan, Department of Biological Chemistry Desviat, Lourdes; Centro de Diagnóstico de Enfermedades Moleculares, Centro de Biología Molecular Ugarte, Magdalena; Centro de Diagnóstico de Enfermedades Moleculares., Centro de Biología Molecular Pérez, Belen; Centro de Diagnóstico de Enfermedades Moleculares., Centro de Biología Molecular
Key Words:	methylmalonic aciduria cbIB type, misfolding mutations, splicing mutations, cobalamin



1  
2  
3  
4  
5  
6  
7  
8  
9  
10  
11  
12  
13  
14  
15  
16  
17  
18  
19  
20  
21  
22  
23  
24  
25  
26  
27  
28  
29  
30  
31  
32  
33  
34  
35  
36  
37  
38  
39  
40  
41  
42  
43  
44  
45  
46  
47  
48  
49  
50  
51  
52  
53  
54  
55  
56  
57  
58  
59  
60

For Peer Review

Humu-2009-0515

Research Article

Supporting Information for this preprint is available from the  
*Human Mutation* editorial office upon request (humu@wiley.com)

## FUNCTIONAL AND STRUCTURAL ANALYSIS OF FIVE MUTATIONS IDENTIFIED IN METHYLMALONIC ACIDURIA *cbIB* TYPE

Ana Jorge-Finnigan<sup>1</sup>, Cristina Aguado<sup>1\*</sup>, Rocio Sánchez-Alcudia<sup>1</sup>, David Abia<sup>2</sup>, Eva Richard<sup>1</sup>, Begoña Merinero<sup>1</sup>, Alejandra Gámez<sup>1</sup>, Ruma Banerjee<sup>3</sup>, Lourdes R. Desviat<sup>1</sup>, Magdalena Ugarte<sup>1</sup> and Belen Pérez<sup>1</sup>

<sup>1</sup>Centro de Diagnóstico de Enfermedades Moleculares, Centro de Biología Molecular-SO UAM-CSIC, Universidad Autónoma de Madrid, Campus de Cantoblanco, 28049 Madrid /Centro de Investigación Biomédica en Red de Enfermedades Raras (CIBERER), ISCIII, Madrid, Spain.

<sup>2</sup> Servicio de Bioinformática, Centro de Biología Molecular-SO UAM-CSIC.

<sup>3</sup> Department of Biological Chemistry, University of Michigan Medical Center, Michigan, USA.

\*Present address: Universidad Pompeu Fabra.

Corresponding author:

Magdalena Ugarte,

Centro de Biología Molecular "Severo Ochoa" CSIC-UAM,

C/ Nicolás Cabrera N° 1,

Universidad Autónoma de Madrid,

1  
2  
3  
4  
5  
6  
7  
8  
9  
10  
11  
12  
13  
14  
15  
16  
17  
18  
19  
20  
21  
22  
23  
24  
25  
26  
27  
28  
29  
30  
31  
32  
33  
34  
35  
36  
37  
38  
39  
40  
41  
42  
43  
44  
45  
46  
47  
48  
49  
50  
51  
52  
53  
54  
55  
56  
57  
58  
59  
60

28049 Madrid,  
Spain.

Phone: +34 91 497 4589

Fax: +34 91 734 7797

E-mail: mugarte@cbm.uam.es

For Peer Review

**ABSTRACT**

ATP:cob(I)alamin adenosyltransferase (ATR, E.C.2.5.1.17) converts reduced cob(I)alamin to the adenosylcobalamin cofactor. Mutations in the *MMAB* gene encoding ATR are responsible for the *cbIB* type methylmalonic aciduria. Here we report the functional analysis of five *cbIB* mutations to determine the underlying molecular basis of the dysfunction. The transcriptional profile along with minigenes analysis revealed that c.584G>A, c.349-1G>C and c.290G>A affect the splicing process. Wild-type ATR and the p.I96T (c.287T>C) and p.R191W (c.571C>T) mutant proteins were expressed in a prokaryote and a eukaryotic expression systems. The p.I96T protein was enzymatically active with a  $K_M$  for ATP and  $K_D$  for cob(I)alamin similar to wild-type enzyme, but exhibited a 40% reduction in specific activity. Both p.I96T and p.R191W mutant proteins are less stable than the wild-type protein, with increased stability when expressed under permissive folding conditions. Analysis of the oligomeric state of both mutants showed a structural defect for p.I96T and also a significant impact on the amount of recovered mutant protein that was more pronounced for p.R191W that, along with the structural analysis, suggest they might be misfolded. These results could serve as a basis for the implementation of pharmacological therapies aimed at increasing the residual activity of this type of mutations.

**Keywords:** methylmalonic aciduria *cbIB* type; ATR; *MMAB*; misfolding; splicing; cobalamina

## INTRODUCTION

ATP:cob(I)alamin adenosyltransferase (ATR, E.C.2.5.1.17) is an enzyme involved in vitamin B<sub>12</sub> metabolism that converts reduced cob(I)alamin to adenosylcobalamin, the active cofactor of methylmalonyl-CoA mutase (MUT, EC 5.4.99.2), which catalyzes the reversible rearrangement of methylmalonyl-CoA to succinyl-CoA in the catabolism of branched-chain amino acids, odd-chain fatty acids and cholesterol. Mutations in the human *MMAB* gene encoding the ATR enzyme are responsible for the *cbIB* type methylmalonic aciduria (MIM# 607568) (Dobson et al., 2002; Leal et al., 2003). *CbIB* patients present either a severe form with neonatal ketoacidosis, lethargy, failure to thrive and encephalopathy or a milder, chronic form with less impaired neurological outcome. A cellular *in vitro* response to hydroxocobalamin (OHCbl) has been reported in certain cases but this response appears to be unclear *in vivo*.

The human *MMAB* gene product, the ATR enzyme, is a member of the PduO family of cobalamin adenosyltransferases, which catalyzes the transfer of adenosine from ATP to cobalamin generating AdoCbl. To date, 24 mutations have been identified in the *MMAB* gene in *cbIB* type patients (HGMD<sup>®</sup> Professional Release 2009.3). Recently, the crystal structures of the homologous ATR proteins from *T. acidophilum* and *L. reuteri* along with the human enzyme with ATP bound have been determined (Saridakis et al., 2004; Schubert and Hill, 2006; St Maurice et al., 2007), allowing for evaluation of the structural impact of pathogenic mutations in ATR. The enzyme is a homotrimer, each subunit composed of a five-helix bundle and an active site located at the subunit interface. Several mutations identified in patients have been mimicked in

1  
2  
3 prokaryotic orthologs and their kinetic parameters determined. They revealed the  
4 existence of mutants with reduced affinity for the substrate and cofactor (p.R191W) and  
5 with negligible activity and presumed instability *in vivo* (p.R186W, p.R190H and  
6 p.E193K) (Zhang et al., 2006). In another study, a *Salmonella* ATR-deficient strain was  
7 used to express mutations generated by random mutagenesis in the human ATR coding  
8 sequence, allowing the delineation of the active site of the enzyme and the putative  
9 residues implicated in cob(II)alamin reduction (Fan and Bobik, 2008).  
10  
11  
12  
13  
14  
15  
16  
17  
18  
19

20 In this study, we report the genetic analysis of four methylmalonic aciduria *cbIB*  
21 type patients and the functional analysis of the identified mutations. In order to  
22 determine the molecular basis of *in vitro* B<sub>12</sub> responsiveness we have functionally  
23 analyzed two missense changes, p.I96T and p.R191W, identified in three B<sub>12</sub>  
24 responsive patient-derived cell lines, in prokaryotic and eukaryotic *in vitro* expression  
25 systems. We have also included the functional analysis of the three mutations affecting  
26 splicing (c.290G>A, c.584G>A and c.349-1G>C) in an *ex vivo* assay using minigenes.  
27  
28  
29  
30  
31  
32  
33  
34  
35  
36  
37  
38

## 39 MATERIALS AND METHODS

### 40 ***Genetic and biochemical analysis in patients' fibroblasts***

41 Patient 1 (P1), previously described in (Merinero et al., 2008), had a neonatal  
42 presentation of the disease. Patients 2 (P2) and 3 (P3) are siblings, P2 developed a late  
43 onset of the disease (at 4 years) and died shortly afterwards. P3 was genetically  
44 diagnosed without presenting clinical symptoms and to date, he is clinically normal.  
45 Patient 4 (P4) was referred to our laboratory for genetic analysis (Table 1). Since  
46 diagnosis, both the asymptomatic patients P3 and P4 are under therapy with protein  
47  
48  
49  
50  
51  
52  
53  
54  
55  
56  
57  
58  
59  
60

1  
2  
3 restriction, carnitine supplementation, OHCbl administration, oral (5ml/d) in P3, and  
4  
5 intramuscular (5mg/15d) in P4 and metronidazol (only P4). During therapy the patients  
6  
7 show differences at the biochemical level: P3 shows milder plasma C3 levels (~10 $\mu$ M)  
8  
9 compared to P4 (80 $\mu$ M); P3 has normal plasma odd-chain fatty-acid levels (OLCFA)  
10  
11 (<0.4%) while P4 has increased ones (~4%). Urine MMA varies in P3 (<200-6000  
12  
13 mmol/mol creat), while there is no data available from P4. P3 has a perfect clinical  
14  
15 development according to the clinician. P4 has a normal neurological and cardiological  
16  
17 evaluation with normal renal function, weight (percentile 25-50) and height  
18  
19 (percentile10) and he is doing well at school. Due to reduction of bone density in lumbar  
20  
21 spine, alandronate, calcium and vitamin D were administered with improvement in  
22  
23 growth and bone density. During his life he has showed some other metabolic  
24  
25 decompensations associated with infections, vomiting, metabolic ketoacidosis etc.  
26  
27 without requiring hospital admission. In these crises the patient required nutritional  
28  
29 adaptation. It is worth noting that the patient has excellent dietary compliance. This work  
30  
31 has been approved by our institutional ethics committee and informed consent has been  
32  
33 obtained from the patients and their legal care-givers.  
34  
35  
36  
37  
38  
39

40  
41 Fibroblast cell lines from patients were cultured under standard conditions in  
42  
43 MEM supplemented with 10% fetal bovine serum, 200 mM glutamine and antibiotics.  
44  
45 Incorporation of radioactivity from [1-<sup>14</sup>C] propionate into acid-precipitable material was  
46  
47 assayed in intact fibroblasts grown in basal medium  $\pm$  1  $\mu$ g/mL OHCbl as previously  
48  
49 described (Perez-Cerda et al., 1989). All data are summarized in Table 1.  
50  
51  
52

53 To identify mutations in the *MMAB* gene, cDNA sequence analysis was  
54  
55 performed. The identified changes were confirmed by sequencing the corresponding  
56  
57  
58  
59  
60

1  
2  
3 genomic DNA region. Genotype analysis was performed using the primers and  
4 conditions described previously (Martinez et al., 2005). Fibroblast cell lines were used  
5 as a source of DNA and RNA, which were isolated using the MagnaPure system  
6 following the manufacturer's protocol (Roche Applied Sciences, Indianapolis, In).  
7  
8 Mutation nomenclature follows the recommended guidelines of the Human Genome  
9 Variation Society (www.HGVS.org). Nucleotide numbering is based on cDNA reference  
10 sequences GenBank accession number NM\_052845.3.  
11  
12  
13  
14  
15  
16  
17  
18  
19  
20  
21

### 22 ***Functional analysis of the splicing mutations***

23  
24 For evaluation of *in vitro* splicing, the pSPL3 vector (Life Technologies, Gibco, BRL,  
25 kindly provided by Dr. B. Andresen, Aarhus University, Denmark) was used. Gene  
26 fragments corresponding to exons and flanking intronic regions were amplified from  
27 patients P2 and P4 and from a DNA control and cloned into the TOPO vector  
28 (Invitrogen, Carlsbad, CA) as previously described (Rincon et al., 2007). 2 µg of the  
29 wild-type or mutant minigenes were transfected into the following cell lines: Hep3B,  
30 HEK293 or COS7 using JetPEI, following the manufacturer's recommendations. 24-48 h  
31 postransfection, cells were harvested, RNA was purified and RT-PCR analysis was  
32 performed using the pSPL3-specific primers SD6 and SA2 (Exon Trapping System,  
33 Gibco, BRL). The identity of amplified bands was determined by sequence analysis.  
34  
35  
36  
37  
38  
39  
40  
41  
42  
43  
44  
45  
46  
47  
48  
49  
50

### 51 ***Prokaryotic and eukaryotic expression analysis of missense changes***

52  
53 Mutation p.I96T (c.287T>C) and p.R191W (c.571C>T) were introduced using the  
54 QuikChange Site Directed Mutagenesis kit (Stratagene, Cedar Drive, TX). The  
55  
56  
57  
58  
59  
60

1  
2  
3 oligonucleotides used for mutagenesis were: *MMAB* I96T sense  
4 (5'AGTTCAGCTACTGGGTTTGCTCTG3'), *MMAB* I96T antisense  
5 (5'CAGAGCAAACCCAGTAGCTGAACT3'), *MMABR191W* sense  
6 (5'CCGTGTGCCGCTGGGCCGAGAGAC3') and *MMAB* R191W antisense  
7 (5'GTCTCTCGGCCAGCGGCACACGG3').  
8  
9  
10  
11  
12  
13  
14

15 For prokaryotic expression analysis we used the NL173 plasmid, based on pET41a,  
16 which contains the human ATR sequence without the mitochondrial targeting sequence.  
17  
18 Human ATR protein was expressed in *E. coli* (BL21Star<sup>TM</sup>DE3 One Shot Cells) and  
19 purified following the method described by (Leal et al., 2004). Bacterial cells were  
20 transformed with the NL173 plasmid encoding either the normal or mutant (p.I96T and  
21 p.R191W) ATRs. Protein expression was induced with 1 mM IPTG; 5 h after induction,  
22 cells were collected by centrifugation and frozen at -70°C until further use. Cell pellets  
23 were resuspended at 4°C in 50 mM potassium phosphate buffer, pH 8, 100 mM NaCl, 1  
24 mM DTT, 1 mM protease inhibitor phenylmethylsulphonyl fluoride, 1 mM EDTA, 0.05  
25 mg/ml DNase, 0.3 mg/ml lysozyme. After 1 h of incubation, the cell suspension was  
26 sonicated and centrifuged to obtain the crude soluble cell extract which was subjected  
27 to ammonium sulphate precipitation and subsequent anion-exchange chromatography  
28 using a Sepharose Q column, as previously described (Leal et al., 2004). In all  
29 purification steps, protein concentration was determined by the Bradford assay.  
30 Fractions eluted from the Sepharose Q column were subjected to SDS-PAGE to identify  
31 those enriched with the ATR protein. In some cases before ATR enzymatic assay, wild-  
32 type and mutant ATR proteins were further purified by hydroxyapatite chromatography  
33 at 4°C using as mobile phase a gradient of 10-400 mM potassium phosphate buffer pH  
34  
35  
36  
37  
38  
39  
40  
41  
42  
43  
44  
45  
46  
47  
48  
49  
50  
51  
52  
53  
54  
55  
56  
57  
58  
59  
60

1  
2  
3 8, and 5 mM KCl. Fractions containing ATR of the highest purity were pooled and  
4  
5 concentrated using an Amicon concentrator to a final concentration of 10 mg/ml.  
6  
7

8  
9 Full-length cDNA of wild-type *MMAB* was generated from total RNA fibroblasts by  
10  
11 RT-PCR and cloned into pGEM-T vector (Promega, Madison, WI). Subsequently, *MMAB*  
12  
13 cDNA was further excised and inserted into HindIII/EcoRV sites of pFLAG-CMV-5c  
14  
15 expression vector (Sigma, St. Louis, MO) to obtain *MMAB* cDNA coupled with FLAG-tag  
16  
17 at the C-terminus (pFLAG-*MMAB*).  
18  
19

20  
21  
22 Eukaryotic expression analysis was performed in the P4 fibroblast cell line stably  
23  
24 transformed with pBABE kindly provided by Dr. JA Enriquez (University of Zaragoza,  
25  
26 Spain). A total of  $4 \times 10^5$  transformed cells were transfected using 2.5  $\mu$ g of normal or  
27  
28 mutant pFLAG-*MMAB* constructs using lipofectamine 2000 (Invitrogen, Carlsbad, CA);  
29  
30 then the cells were grown at 27 or 37° C. Harvested cells were used to determine ATR  
31  
32 activity which was indirectly measured by the analysis of [<sup>14</sup>C]-propionate incorporation  
33  
34 into acid-precipitable material in intact cells grown in basal medium (Perez-Cerda et al.,  
35  
36 1989) Propionate oxidation is catalyzed by two mitochondrial enzymes, the biotin-  
37  
38 dependent propionyl-CoA carboxylase and the AdoCbl-dependent methylmalonyl-CoA  
39  
40 mutase. AdoCbl is synthesized by ATR and the patients with defects in the *MMAB* gene  
41  
42 exhibit deficient propionate incorporation. Statistical analysis was performed using an *F*-  
43  
44 test analysis of variance followed by a 1-tailed paired *t*-test. P values less than 0.05  
45  
46 were considered significant.  
47  
48  
49  
50  
51

### 52 53 54 55 **Enzyme activity assays** 56 57 58 59 60

1  
2  
3 ATR activity was measured as previously published (Johnson et al., 2001) with  
4  
5 minor modifications. Assays contained 200 mM Tris-HCl pH 8.0, 1.6 mM KH<sub>2</sub>PO<sub>4</sub>, 2.8  
6  
7 mM MgCl<sub>2</sub>, 100 mM KCl, 0.4 mM ATP and 80 μM OHCbl (Sigma Aldrich, St. Louis,  
8  
9 MO). 800 μl aliquots of the reaction mixture were dispensed into cuvettes kept at 37°C.  
10  
11 Titanium (III) citrate (10 μl) was added, the reaction initiated by the addition of 10-100  
12  
13 μg of purified protein, and the decrease in absorbance at 388 nm was monitored.  
14  
15 Anaerobic procedures were used to prepare the reaction mix, the protein solution and  
16  
17 titanium(III)citrate.  
18  
19  
20  
21  
22  
23

### 24 ***Measurement of dissociation constants***

25  
26 The equilibrium dissociation constants (K<sub>d</sub>) for cob(II)alamin analogs were determined  
27  
28 fluorimetrically as described by (Chowdhury and Banerjee, 1999) with modifications. To  
29  
30 determine the K<sub>d</sub> values, 40-150 μg of protein in 50 mM Tris-HCl buffer, pH 8.0, was  
31  
32 added to a quartz cuvette and successive aliquots (1-10 μl) of the cobalamin analogue  
33  
34 (2-7 mM) were added then the fluorescence (excitation wavelength: 280 nm, emission  
35  
36 wavelength 340 nm) was measured after each addition. The K<sub>d</sub> for cob(II)alamin was  
37  
38 determined under anaerobic conditions by monitoring the shift in the UV-visible  
39  
40 spectrum from 300 nm to 750 nm using 10 μM cob(II)alamin and varying concentrations  
41  
42 of ATR as described previously (Yamanishi et al., 2005). The kinetic data were  
43  
44 analyzed using the IGOR Pro6 software (WaveMetrics Inc, Lake Oswego, OR).  
45  
46  
47  
48  
49  
50  
51  
52  
53  
54

### 55 ***Western blot analysis***

56  
57  
58  
59  
60

1  
2  
3  
4 Protein concentration in fibroblast and bacterial cell extracts was determined using  
5 the BIO-RAD protein assay (Bio-Rad, Bio-Rad Laboratories, Munchen, Germany)  
6 following the manufacturer's protocol. Equal amounts of total protein for bacterial cell  
7 extracts were loaded onto a 10% Laemmli SDS-PAGE System. After SDS-PAGE or  
8 native gel electrophoresis, proteins were transferred to a nitrocellulose transfer  
9 membrane (GE Healthcare, Buckinghamshire, UK) using a BIO-RAD apparatus in Tris  
10 (25 mM)-glycine (192 mM)-methanol (20%) without SDS for 1 h. Poinceau staining was  
11 used to monitor equal loading of protein. Immunodetection was carried out using  
12 commercially available anti-ATR antibodies (ProteinTech Group Inc, Chicago, IL) as  
13 primary antibodies diluted 1:1000. The secondary antibodies used were conjugated  
14 goat-anti mouse IgG-horseradish peroxidase (1:10000) (Santa Cruz Biotechnology Inc,  
15 Santa Cruz, CA) and were detected using the Enhanced Chemiluminescence System  
16 (GE Healthcare, Buckinghamshire, UK). Relative protein amounts were determined  
17 using a calibrated densitometer GS-800 (BioRad).  
18  
19  
20  
21  
22  
23  
24  
25  
26  
27  
28  
29  
30  
31  
32  
33  
34  
35  
36  
37  
38  
39

### ***Oligomeric state of ATR***

40  
41 Size-exclusion chromatography using a Superdex 200 (1.2 cm x 92 cm) column  
42 was performed to assess the oligomeric state of the wild-type and mutant ATR proteins.  
43 100 µg of protein purified by ammonium sulphate precipitation and anion-exchange  
44 chromatography were applied to the column in 50 mM Tris HCl buffer pH 8.0, 100 mM  
45 KCl and a flow rate of 2.0 ml min<sup>-1</sup>. Molecular mass value estimations were obtained  
46 using a calibration curve generated with molecular weight standards (Bio-Rad).  
47  
48  
49  
50  
51  
52  
53  
54  
55  
56  
57  
58  
59  
60

1  
2  
3 Blue native electrophoresis was performed using 4-16% Native PAGE gels, Native  
4 Marker and Native running buffer from Invitrogen. Samples were prepared with 4x  
5 Native sample buffer with G-250 sample additive (Invitrogen). The electrophoretic  
6 separation was performed at 4°C for one hour at 150V followed by another hour at  
7 250V. Lanes containing purified ATR and molecular weight marker were stained using  
8 2% Coomassie Brilliant Blue R-250 (Bio-Rad) solution in acetic acid and destained in  
9 acetic acid: methanol: water (0.5:2:2). The remaining lanes were transferred to a PVDF  
10 membrane using the iBLOT system from Invitrogen. Immunodetection was carried out  
11 as described above.  
12  
13  
14  
15  
16  
17  
18  
19  
20  
21  
22  
23

### 24 25 26 27 ***Protein stability studies***

28  
29 The stability of the wild-type and mutant p.I96T and p.R191W proteins expressed  
30 in the prokaryotic system was investigated by incubating the transformed cells at 37°C  
31 or 27°C following IPTG induction. Soluble supernatant was incubated at 37 or 27°C,  
32 aliquots were removed at different time points and the cell extracts were subjected to  
33 SDS-PAGE. Western blot analysis was performed as described above. Following  
34 densitometric analysis, relative protein levels were expressed as percentage referred to  
35 time 0.  
36  
37  
38  
39  
40  
41  
42  
43  
44  
45  
46  
47

### 48 49 ***Structural analysis and molecular dynamics***

50 Visualization of the crystal structure of ATR and localization of the mutant residue I96  
51 was performed using DSViewerPro5.0 (Accelrys Inc, San Diego, CA) with the PDB  
52 coordinates file 2IDX.  
53  
54  
55  
56  
57  
58  
59  
60

1  
2  
3 Human ATP:cobalamin adenosyltransferase (hATR) monomers were modelled  
4 using as template, the B and C chains from the PDB structure 2IDX (Schubert and Hill,  
5 2006), and the program MODELLER9v7 (Eswar et al., 2006). The ATP binding loop  
6 'KIYTK' was kept in the bound conformation from chain B, while the unresolved loop  
7 'SSAREAHLKYT' in B chain was taken from C chain. Trimer reconstruction was  
8 performed by superposition of the modelled monomer over 2IDX structure with the help  
9 of the MAMMOTH program (Ortiz et al., 2002). All three active sites were modelled as  
10 occupied by an ATP molecule.  
11  
12  
13  
14  
15  
16  
17  
18  
19  
20  
21

22 Models of mutants p.R191W and p.I96T were generated with the program  
23 PyMOL (DeLano, 1998-2003) using the modelled trimer as template. Protonation states  
24 of ionizable groups at pH 6.5 for the three systems were calculated using the H++  
25 server (Gordon et al., 2005). The positions of hydrogen atoms, standard atomic charges  
26 and radii for all the atoms were assigned according to the ff03 force field (Duan et al.,  
27 2003). The complexes were immersed in cubic boxes of TIP3P water molecules  
28 (William et al., 1983) large enough to guarantee that the shortest distance between the  
29 solute and the edge of the box was larger than 13 Å. Counter ions were also added to  
30 maintain electro neutrality. Three consecutive minimizations were performed involving:  
31 i) only hydrogen atoms; ii) only the water molecules and ions; and iii) the entire system.  
32  
33  
34  
35  
36  
37  
38  
39  
40  
41  
42  
43  
44  
45  
46  
47

### 48 ***Simulation details***

49 Starting minimized structures, prepared as stated above, were simulated in the  
50 NPT ensemble using Periodic Boundary Conditions and Particle Mesh Ewald to treat  
51 long-range electrostatic interactions. The systems were then heated and equilibrated in  
52  
53  
54  
55  
56  
57  
58  
59  
60

1  
2  
3 two steps: i) 200 ps of molecular dynamics (MD) heating the whole system from 100 K  
4 to 300 K, and ii) equilibration of the entire system during 1.0 ns at 300 K. The  
5  
6 equilibrated structures were the starting points for the 15 ns MD simulations at constant  
7  
8 temperature (300 K) and pressure (1 atm). SHAKE algorithm was used to keep bonds  
9  
10 involving H atoms at their equilibrium length, allowing a 2 fs time step for the integration  
11  
12 of Newton's equations of motion. ff03 and TIP3P force fields, as implemented in  
13  
14 AMBER 10 package (D.A. Case, 2008), were used to describe the proteins, the  
15  
16 peptides and the water molecules, respectively. Sample frames at 10 ps intervals from  
17  
18 the molecular dynamics trajectory were subsequently used for the analysis.  
19  
20  
21  
22  
23  
24  
25  
26

### 27 ***In silico stability analysis***

28  
29 Absolute free energies of the hATR complex and its mutants (p.R191W and  
30  
31 p.I96T) were estimated using the MM-GBSA (Still et al., 2002) approach as  
32  
33 implemented in the AMBER10 package. MM-GBSA method approaches the free energy  
34  
35 of the complexes as a sum of a molecular mechanic (MM) interaction term, a solvation  
36  
37 contribution through a generalized Born (GB) model, and a surface area (SA)  
38  
39 contribution to account for the non-polar part of solvation. Distributions of the observed  
40  
41 free energies, measured every 10 ps snapshots along with the molecular dynamics  
42  
43 simulations, were plotted using the R package (Gentleman R., 1997).  
44  
45  
46  
47

48 In addition, to better characterize the changes produced by the mutated  
49  
50 residues, an energy decomposition analysis in a pairwise fashion (between the residues  
51  
52 surrounding the mutations) was performed using a cut off of 5 Å from the mutated  
53  
54 residues. Polar contribution to solvation free energies were calculated with GB, whereas  
55  
56  
57  
58  
59  
60

1  
2  
3 non-polar contributions were estimated to be proportional to the area lost upon binding  
4  
5 using the LCPO method to calculate accessible surface areas (Weiser et al., 1999).  
6  
7

8 These calculations were performed, for each 10 ps snapshot from the  
9  
10 simulations, using the appropriate module within AMBER 10 package. Free energy  
11  
12 decomposition interaction matrix was represented in an energy dependent colour  
13  
14 gradient using the program matrix2png (Pavlidis and Noble, 2003).  
15  
16  
17

## 18 19 20 **RESULTS**

21  
22 P1, P2 and P4 patients showed normal MUT activity and P1 and P2 exhibited *in*  
23  
24 *vitro* responsiveness to B<sub>12</sub> (Table 1). The age of onset and the clinical outcome of  
25  
26 these patients are summarized in Table 1. The p.I96T (c.287T>C) sequence change  
27  
28 was identified in three of the patients (Patients P1, P2 and P3). This mutation was found  
29  
30 in combination with the missense change p.R191W (c.571C>T) and in two siblings in  
31  
32 combination with c.584G>A mutation, affecting the last nucleotide of exon 7 in the  
33  
34 *MMAB* gene. This last mutation results in exon 7 skipping (r.520\_584del) in patient  
35  
36 fibroblasts, which would result in a premature stop codon (p.S174fs) (Figure 1A).  
37  
38  
39

40  
41 The RT-PCR pattern and subsequent sequence analysis of the amplified  
42  
43 products obtained from patient P4 fibroblasts, showed the presence of two bands, one  
44  
45 of them corresponding to the skipping of exon 3 (r.197\_290del), which is predicted to  
46  
47 generate a truncated protein and the other one corresponding to an in-frame deletion of  
48  
49 two amino acids (r.349\_354del6, p.I117\_Q118del) due to activation of a cryptic splice  
50  
51 site inside exon 5. The genomic DNA analysis showed two nucleotide changes  
52  
53  
54  
55  
56  
57  
58  
59  
60

1  
2  
3 c.290G>A and c.349-1G>C in the last nucleotide of exon 3 and in the 3' splice site of  
4  
5  
6 intron 4, respectively (Figure 1B).  
7  
8  
9

### 10 ***Functional analysis of the splicing mutations***

11  
12 In this work, we have investigated the functional effect of the three nucleotide  
13 changes affecting splicing (c.290G>A, c.349-1G>C and c.584G>A) using a cell based  
14  
15 splicing assay. In the patient fibroblasts, only transcripts resulting from the skipping of  
16  
17 exon 7 and exon 3 derived from the c.584G>A and c.290G>A alleles are detected.  
18  
19 However, if correct splicing occurred occasionally, a mutant protein with the p.R195H  
20  
21 and p.G97E changes would result. A minigene functional splicing assay was employed  
22  
23 to investigate this possibility. All splicing mutations were cloned in minigenes and  
24  
25 transfected in Hep3B, HEK293 or COS cells. All the mutants resulted in aberrant  
26  
27 splicing. In addition of the strong 3' and 5' splice sites, the pSPL3 vector has after the  
28  
29 multiple cloning site, cryptic 3' and 5' splice sites. In the case of the c.290G>A and  
30  
31 c.584G>A mutant constructs, both splicing sequences were used, the classical and the  
32  
33 cryptic one and therefore the fragment amplified contained a vector sequence  
34  
35 generated from use of the weaker cryptic splice sites (Figure 2) In the case of c.584G>A  
36  
37 a small but detectable amount of the correctly spliced transcript (resulting in the  
38  
39 p.R195H change) was observed.  
40  
41  
42  
43  
44  
45  
46  
47  
48  
49  
50

### 51 ***Functional and structural analysis of the missense mutations***

52  
53 Since the three patients responsive to B<sub>12</sub> *in vitro* share the p.I96T mutation  
54  
55 described previously (Merinero et al., 2008), we sought to analyze the kinetic stability  
56  
57  
58  
59  
60

1  
2  
3 properties of the mutant protein. Residue I96 is located in helix  $\alpha$ 1 (Figure 3A), distant  
4 from the ATP binding site while residue R191 projects into the central cavity of the  
5 trimeric protein. Given the location of the I96 residue in  $\alpha$ 1 helix, the mutation could  
6 change the stability of the protein and/or perturb binding of the substrates, ATP and  
7 cobalamin but is not predicted to be involved in trimer formation.  
8  
9

10  
11 Absolute free energies for wild-type hATR and the mutants, p.R191W and p.I96T,  
12 were estimated by the MM-GBSA method and predicted a decrease in stability for the  
13 p.R191W mutant ( $-15026.93 \pm 68.35$  kcal/mol) compared to the wild-type ATR ( $-$   
14  $15436.88 \pm 72.76$  kcal/mol) or the p.I96T mutant ( $-15441.07 \pm 67.06$  kcal/mol). In fact, a  
15 significant difference was not found between wild-type ATR and the p.I96T mutant  
16 (Supp. Figure S1).  
17  
18  
19  
20  
21  
22  
23  
24  
25  
26  
27  
28

29 In addition, pair wise interaction energies were calculated for the residues  
30 surrounding the mutations. In p.R191W, a network of hydrogen bonds at the trimer  
31 centre involving R191 and E91 residues was detected, linking the three monomers  
32 (Figure 3B). The equivalent interaction in p.R191W mutant is substantially diminished  
33 (Figure 3C). However, this energy loss is compensated, at least in part, by a new inter  
34 subunit hydrogen bond pattern established between the R190 and E91 residues. In  
35 addition, the effect of the stacked conformation adopted by the mutant W191 residue  
36 creates a distortion in the trimer core that is reflected by other changes involving the  
37 interaction profile of E84, especially those related to R194 and R195, and the interaction  
38 between R190 and bound ATP (data not shown). On the contrary, a significant  
39 difference in the pair wise interaction energy when comparing I96T mutant to the wild-  
40 type protein was not observed.  
41  
42  
43  
44  
45  
46  
47  
48  
49  
50  
51  
52  
53  
54  
55  
56  
57  
58  
59  
60

1  
2  
3 Wild-type and mutant (p.I96T) ATR were expressed in *E. coli* and purified. The  
4 degree of purification was estimated to be 95% after the first step and ~99% after the  
5 final step. The specific activity and kinetic parameters for wild-type and p.I96T ATR  
6 were measured in parallel (Table 2) and similar results were obtained with and without  
7 the last hydroxyapatite purification step. The p.I96T mutant exhibits a slight reduction in  
8 specific activity, retaining 60% of wild-type levels with no significant differences in the  
9 Kds for ATP or cobalamins, with the exception of CNCbl which showed a 1.7-fold  
10 increase in Kd.  
11  
12  
13  
14  
15  
16  
17  
18  
19  
20  
21

22 The oligomeric profile of the p.I96T mutant protein was analyzed by size  
23 exclusion chromatography following ammonium sulphate precipitation and anion-  
24 exchange chromatography. Under these conditions, the protein exists mainly as a  
25 trimeric, similar to wild-type ATR (data not shown). Electrophoresis under  
26 nondenaturing conditions detected aggregates of ATR in the crude cell lysates  
27 (supernatants or pellets) with either wild-type or mutant ATR, although the size  
28 distributions were different (Figure 4). Wild-type ATR showed lower molecular weight  
29 aggregates (~250 kDa), while the majority of the protein was present in a trimeric form.  
30 The p.I96T mutant showed both trimeric and monomeric forms. Both supernatant and  
31 crude extracts of mutant proteins showed a significant reduction in the amount of  
32 protein recovered, more pronounced in the case of p.R191W that could not be detected  
33 under any conditions (Figure 4).  
34  
35  
36  
37  
38  
39  
40  
41  
42  
43  
44  
45  
46  
47  
48  
49

50 Next, we investigated the relative stabilities of the p.I96T and p.R191W mutants  
51 expressed in bacteria grown at 37°C or 27°C (Figure 5). The p.I96T mutant was found  
52 to have a significantly decreased half life (Figure 5A) compared to wild-type protein at  
53  
54  
55  
56  
57  
58  
59  
60

1  
2  
3 37°C (34 versus 85 h). At lower temperature (27°C) the half-lives for both proteins  
4  
5 increased (Figure 5B).  
6  
7

8 R191 projects into the central cavity of the trimeric ATR structure (Figure 3A);  
9  
10 interactions between this residue from adjacent monomers might play a role in  
11  
12 stabilizing the quaternary structure of the protein. In fact, the p.R191W mutant was  
13  
14 highly unstable at 37°C (Figure 5A) with a half-life of 1.3 h. The expression level of the  
15  
16 mutant increased when the cells were grown at 27°C with a corresponding increase in  
17  
18 its half-life to 26.5 h (Figure 5B).  
19  
20  
21

22 Wild-type and mutant ATRs were also expressed as fusion proteins with a FLAG  
23  
24 tag in a *cbIB* fibroblast cell line (P4). Cells were cultured at 37°C and 27°C and the [<sup>14</sup>C]-  
25  
26 propionate incorporation levels were determined as an indirect measure of ATR activity  
27  
28 in the transfected cells. At 37°C, the mutant p.I96T and p.R191W proteins showed a  
29  
30 statistically significant reduction in [<sup>14</sup>C]-propionate incorporation: 65% and 52% of wild-  
31  
32 type levels respectively. When the cells were grown at 27°C, [<sup>14</sup>C]-propionate  
33  
34 incorporation levels of p.I96T and p.R191W mutants increased to levels close to wild-  
35  
36 type ones (Figure 6).  
37  
38  
39  
40  
41  
42  
43  
44  
45

## 46 DISCUSSION

47  
48 The focus of this work was the functional analysis of five *cbIB* mutations and the  
49  
50 investigation of the underlying molecular mechanism of *in vitro* B<sub>12</sub> responsiveness  
51  
52 observed in three MMA patients belonging to the *cbIB* class. The results obtained  
53  
54 indicate that all five nucleotide changes are disease-causing mutations, opening the  
55  
56  
57  
58  
59  
60

1  
2  
3 possibility for genetic counselling, carrier identification and prenatal diagnosis in at-risk  
4 families, and allowing determination of possible phenotype-genotype correlations and  
5 mutation-specific therapies.  
6  
7  
8  
9

10 Regarding the functional analysis of the exonic and intronic nucleotide changes  
11 affecting splicing, our results suggest that there are negligible levels of normal transcript  
12 associated with the mutations studied, from fibroblasts from patients and in cell lines  
13 (Hep3B, Hek293 and COS cells) transfected with the corresponding minigenes. Based  
14 on our data, the *in vitro* responsiveness in these patients might be associated with the  
15 missense changes, p.I96T or p.R191W. In relation to patient P4 who bears two splicing  
16 mutations, no stimulation of [<sup>14</sup>C]-propionate was observed when cells were  
17 supplemented with OHCbl. However, given that the patient is clinically asymptomatic,  
18 the in-frame deletion of two amino acids resulting from the c.349-1G>C allele might  
19 retain certain degree of activity. Addressing this will be the aim of future investigations.  
20  
21  
22  
23  
24  
25  
26  
27  
28  
29  
30  
31  
32  
33

34 The three *in vitro* B<sub>12</sub> responsive patients (P1, P2 and P3) share the missense  
35 mutation p.I96T, which was expressed in a prokaryotic system in order to analyze its  
36 structural and kinetic properties. The mutant protein showed a modest reduction in  
37 specific activity but normal binding affinity for ATP and cob(II)alamin substrates.  
38 Inconsistent results were obtained in evaluating the effect of the mutations on the  
39 oligomeric structure of the protein. Thus, size exclusion chromatography revealed a  
40 normal oligomeric profile, while native gel electrophoresis indicated an aberrant profile.  
41 In the former case, the purification of ATR prior to Superdex chromatography might  
42 have led to the separation of monomers, while the soluble or crude extracts loaded on  
43 the native gel allowed detection of all the ATR forms and involved only minor  
44  
45  
46  
47  
48  
49  
50  
51  
52  
53  
54  
55  
56  
57  
58  
59  
60

1  
2  
3 manipulation. However, the significantly lower levels of mutant protein observed by  
4 native gel electrophoresis, and the lower stability suggests that loss of biological  
5 function in the p196T mutant might be due to abnormal folding rather than a change in  
6 oligomeric state. Impaired protein folding can enhance degradation (e.g. in Gaucher and  
7 lysosomal storage disorders), lead to deposition of misfolded protein (e.g. in Alzheimer's  
8 disease) or result in an inactive form (Majtan et al. in press ; Gamez et al., 2000).  
9

10  
11 When both mutant proteins are expressed in *E. coli* under permissive low  
12 temperature conditions, the steady-state levels of ATR and its half-life are increased.  
13 Similar results were obtained using a eukaryotic expression system where the level of  
14 <sup>14</sup>C-propionate incorporation was similar to control values when the transfected cells  
15 were grown at 27°C. Expression studies of the p.R191W mutation in *E. coli* have been  
16 previously described using a GST fusion protein in which its stability was not mentioned  
17 (Zhang et al., 2006). In contrast, in *Salmonella enterica*, the p.R191W mutant was  
18 expressed at lower levels than the control, indicating that it impairs proper folding and  
19 leads to degradation mediated by cellular proteases (Fan and Bobik, 2008). The  
20 residual activity associated with the pR191W mutant was reported to be 30% in the *E.*  
21 *coli* system and undetectable in *S. enterica* (Fan and Bobik, 2008; Zhang et al., 2006).  
22 Mutations affecting residues close to the 191 position, e.g. R190H and p.E193K are  
23 also unstable in all expression systems (Fan and Bobik, 2008; Zhang et al., 2006) and  
24 might represent a region critical for stability.  
25  
26  
27  
28  
29  
30  
31  
32  
33  
34  
35  
36  
37  
38  
39  
40  
41  
42  
43  
44  
45  
46  
47  
48  
49

50 Our data suggest that p.R191W and p.196T mutants result in severe folding  
51 problems although when expressed as fusion proteins with the Flag peptide in an  
52 eukaryotic expression system, residual activity was observed. However, since transient  
53  
54  
55  
56  
57  
58  
59  
60

1  
2  
3 expression was performed using the P4 cell line, it is possible that in addition to FLAG  
4 stabilization, complementation with the endogenous ATR might have contributed to the  
5 rather high residual activity of these mutants.  
6  
7  
8  
9

10 The responsiveness to *in vitro* OHCbl supplementation could be explained  
11 partially by a stabilizing effect of the cofactor which could act as a natural chaperone, as  
12 has been described for other cofactors, e.g. tetrahydrobiopterin in phenylalanine  
13 hydroxylase deficiency (Erlandsen et al., 2004; Perez et al., 2005; Pey et al., 2004).  
14  
15 Other mechanisms may also be operating in the OHCbl-responsive cell line, P1, since  
16 the p.R191W mutant (albeit with a GST tag) exhibits a 16-fold higher  $K_M$  for cobalamin  
17 (Zhang et al., 2006). Defects in ATR might also affect its interaction with MMAA or MUT  
18 proteins, assuming that the three enzymes operate in a complex and increased levels of  
19  $B_{12}$  might have an stabilizing effect (Banerjee, 2006; Banerjee et al., 2009).  
20  
21  
22  
23  
24  
25  
26  
27  
28  
29  
30  
31

32 In addition to the genetic diagnosis of the disease, knowledge of the mutational  
33 spectrum in each population provides insights into genotype-phenotype correlations.  
34 Based on the clinical outcome, patients bearing the p.I96T mutation exhibit a highly  
35 variable phenotype. Thus, while one of them is clinically asymptomatic, the other two  
36 are either dead or severely neurologically impaired. These findings also suggest that the  
37 missense changes, p.I96T and p.R191W, might be categorized as a loss-of-function  
38 folding mutations that are usually associated with variable genotype-phenotype  
39 correlation (Andresen et al., 1997; Pey et al., 2003; Pey et al., 2007). Inter-individual  
40 differences in gene expression of the protein quality control and proteasomal proteins  
41 have been described as phenotypic modifiers in several misfolding diseases (Dipple  
42 and McCabe, 2000a; Dipple and McCabe, 2000b).  
43  
44  
45  
46  
47  
48  
49  
50  
51  
52  
53  
54  
55  
56  
57  
58  
59  
60

1  
2  
3  
4  
5  
6  
7  
8  
9  
10  
11  
12  
13  
14  
15  
16  
17  
18  
19  
20  
21  
22  
23  
24  
25  
26  
27  
28  
29  
30  
31  
32  
33  
34  
35  
36  
37  
38  
39  
40  
41  
42  
43  
44  
45  
46  
47  
48  
49  
50  
51  
52  
53  
54  
55  
56  
57  
58  
59  
60

In conclusion, functional analysis of the mutations described in this study is relevant to our understanding of the pathogenic mechanisms of MMA and also for the design of mutation-specific therapies. In several genetic disorders such as phenylketonuria or Gaucher's disease (Bernier et al., 2004; Mu et al., 2008; Pey et al., 2008) pharmacological rescue of folding mutants or up-regulation of gene expression for mutants with residual activity is currently envisaged as a possible option for correcting, at least partially, the phenotype. In the case of the p.I96T and p.R191W mutant proteins, pharmacological chaperones or compounds such as statins (Murphy et al., 2007) which may result in activation of *MMAB* gene expression, should be explored as potential strategies to treat the disease if increased steady-state levels and activity of the protein can be achieved.

## ACKNOWLEDGMENTS

Ana Jorge-Finnigan is funded by Fondo de Investigaciones Sanitarias. This work was supported by grants from *Comisión Interministerial de Ciencia y Tecnología* (SAF2007-61350), *Fondo de Investigaciones Sanitarias* (PI060512) and the National Institutes of Health (DK45776). An institutional grant from the *Fundación Ramón Areces* to the Centro de Biología Molecular Severo Ochoa is gratefully acknowledged. We acknowledge the generous allocation of computer time at the Barcelona Supercomputing Center.

**REFERENCES**

- 1  
2  
3  
4  
5  
6  
7  
8  
9  
10  
11  
12  
13  
14  
15  
16  
17  
18  
19  
20  
21  
22  
23  
24  
25  
26  
27  
28  
29  
30  
31  
32  
33  
34  
35  
36  
37  
38  
39  
40  
41  
42  
43  
44  
45  
46  
47  
48  
49  
50  
51  
52  
53  
54  
55  
56  
57  
58  
59  
60
- Andresen BS, Bross P, Udvari S, Kirk J, Gray G, Kmoch S, Chamoles N, Knudsen I, Winter V, Wilcken B and others. 1997. The molecular basis of medium-chain acyl-CoA dehydrogenase (MCAD) deficiency in compound heterozygous patients: is there correlation between genotype and phenotype? *Hum Mol Genet* 6(5):695-707.
- Banerjee R. 2006. B12 trafficking in mammals: A for coenzyme escort service. *ACS Chem Biol* 1(3):149-59.
- Banerjee R, Gherasim C, Padovani D. 2009. The tinker, tailor, soldier in intracellular B12 trafficking. *Curr Opin Chem Biol* 13(4):477-84.
- Bernier V, Lagace M, Bichet DG, Bouvier M. 2004. Pharmacological chaperones: potential treatment for conformational diseases. *Trends Endocrinol Metab* 15(5):222-8.
- Chowdhury S, Banerjee R. 1999. Role of the dimethylbenzimidazole tail in the reaction catalyzed by coenzyme B12-dependent methylmalonyl-CoA mutase. *Biochemistry* 38(46):15287-94.
- D.A. Case TAD, T.E. Cheatham, III, C.L. Simmerling, J. Wang, R.E. Duke, R. Luo, M. Crowley, Ross C. Walker, W. Zhang, K.M. Merz, B.Wang, S. Hayik, A. Roitberg, G. Seabra, I. Kolossváry, K.F.Wong, F. Paesani, J. Vanicek, X.Wu, S.R. Brozell, T. Steinbrecher, H. Gohlke, L. Yang, C. Tan, J. Mongan, V. Hornak, G. Cui, D.H. Mathews, M.G. Seetin, C. Sagui, V. Babin, and P.A. Kollman. 2008. AMBER 10.

- 1  
2  
3 DeLano WL. 1998-2003. The PyMOL Molecular Graphics System. Version 0.93. San  
4 Carlos, CA, USA: DeLano Scientific LLC.  
5  
6  
7  
8 Dipple KM, McCabe ER. 2000a. Modifier genes convert "simple" Mendelian disorders to  
9 complex traits. *Mol Genet Metab* 71(1-2):43-50.  
10  
11  
12 Dipple KM, McCabe ER. 2000b. Phenotypes of patients with "simple" Mendelian  
13 disorders are complex traits: thresholds, modifiers, and systems dynamics. *Am J*  
14 *Hum Genet* 66(6):1729-35.  
15  
16  
17  
18  
19 Dobson CM, Wai T, Leclerc D, Kadir H, Narang M, Lerner-Ellis JP, Hudson TJ,  
20 Rosenblatt DS, Gravel RA. 2002. Identification of the gene responsible for the  
21 *cb1B* complementation group of vitamin B12-dependent methylmalonic aciduria.  
22 *Hum Mol Genet* 11(26):3361-9.  
23  
24  
25  
26  
27  
28  
29 Duan Y, Wu C, Chowdhury S, Lee MC, Xiong G, Zhang W, Yang R, Cieplak P, Luo R,  
30 Lee T and others. 2003. A point-charge force field for molecular mechanics  
31 simulations of proteins based on condensed-phase quantum mechanical  
32 calculations. *J Comput Chem* 24(16):1999-2012.  
33  
34  
35  
36  
37  
38  
39 Erlandsen H, Pey AL, Gamez A, Perez B, Desviat LR, Aguado C, Koch R, Surendran S,  
40 Tying S, Matalon R and others. 2004. Correction of kinetic and stability defects  
41 by tetrahydrobiopterin in phenylketonuria patients with certain phenylalanine  
42 hydroxylase mutations. *Proc Natl Acad Sci U S A* 101(48):16903-8.  
43  
44  
45  
46  
47  
48 Eswar N, Webb B, Marti-Renom MA, Madhusudhan MS, Eramian D, Shen MY, Pieper  
49 U, Sali A. 2006. Comparative protein structure modeling using Modeller. *Curr*  
50 *Protoc Bioinformatics* Chapter 5:Unit 5 6.  
51  
52  
53  
54  
55  
56  
57  
58  
59  
60

- 1  
2  
3 Fan C, Bobik TA. 2008. Functional characterization and mutation analysis of human  
4  
5 ATP:Cob(I)alamin adenosyltransferase. *Biochemistry* 47(9):2806-13.  
6  
7  
8 Gamez A, Perez B, Ugarte M, Desviat LR. 2000. Expression analysis of  
9  
10 phenylketonuria mutations: effect on folding and stability of the phenylalanine  
11  
12 hydroxylase protein. *J Biol Chem* 275:29737-29742.  
13  
14  
15 Gentleman R. IR. 1997. R. Version 2.9.2: The R Foundation for Statistical Computing.  
16  
17  
18 Gordon JC, Myers JB, Folta T, Shoja V, Heath LS, Onufriev A. 2005. H++: a server for  
19  
20 estimating pKas and adding missing hydrogens to macromolecules. *Nucleic*  
21  
22 *Acids Res* 33(Web Server issue):W368-71.  
23  
24  
25 Johnson CL, Pechonick E, Park SD, Havemann GD, Leal NA, Bobik TA. 2001.  
26  
27 Functional genomic, biochemical, and genetic characterization of the *Salmonella*  
28  
29 pduO gene, an ATP:cob(I)alamin adenosyltransferase gene. *J Bacteriol*  
30  
31 183(5):1577-84.  
32  
33  
34 Leal NA, Olteanu H, Banerjee R, Bobik TA. 2004. Human ATP:Cob(I)alamin  
35  
36 adenosyltransferase and its interaction with methionine synthase reductase. *J*  
37  
38 *Biol Chem* 279(46):47536-42.  
39  
40  
41 Leal NA, Park SD, Kima PE, Bobik TA. 2003. Identification of the human and bovine  
42  
43 ATP:Cob(I)alamin adenosyltransferase cDNAs based on complementation of a  
44  
45 bacterial mutant. *J Biol Chem* 278(11):9227-34.  
46  
47  
48 Majtan T, Liu L, Carpenter JF, Kraus JP. Rescue of cystathionine beta-synthase (CBS)  
49  
50 mutants with chemical chaperones: purification and characterization of eight CBS  
51  
52 mutant enzymes. *J Biol Chem*.  
53  
54  
55  
56  
57  
58  
59  
60

- 1  
2  
3  
4  
5  
6  
7  
8  
9  
10  
11  
12  
13  
14  
15  
16  
17  
18  
19  
20  
21  
22  
23  
24  
25  
26  
27  
28  
29  
30  
31  
32  
33  
34  
35  
36  
37  
38  
39  
40  
41  
42  
43  
44  
45  
46  
47  
48  
49  
50  
51  
52  
53  
54  
55  
56  
57  
58  
59  
60
- Martinez MA, Rincon A, Desviat LR, Merinero B, Ugarte M, Perez B. 2005. Genetic analysis of three genes causing isolated methylmalonic acidemia: identification of 21 novel allelic variants. *Mol Genet Metab* 84(4):317-25.
- Merinero B, Perez B, Perez-Cerda C, Rincon A, Desviat LR, Martinez MA, Sala PR, Garcia MJ, Aldamiz-Echevarria L, Campos J and others. 2008. Methylmalonic acidemia: examination of genotype and biochemical data in 32 patients belonging to mut, cblA or cblB complementation group. *J Inherit Metab Dis* 31(1):55-66.
- Mu TW, Ong DS, Wang YJ, Balch WE, Yates JR, 3rd, Segatori L, Kelly JW. 2008. Chemical and biological approaches synergize to ameliorate protein-folding diseases. *Cell* 134(5):769-81.
- Murphy C, Murray AM, Meaney S, Gafvels M. 2007. Regulation by SREBP-2 defines a potential link between isoprenoid and adenosylcobalamin metabolism. *Biochem Biophys Res Commun* 355(2):359-64.
- Ortiz AR, Strauss CE, Olmea O. 2002. MAMMOTH (matching molecular models obtained from theory): an automated method for model comparison. *Protein Sci* 11(11):2606-21.
- Pavlidis P, Noble WS. 2003. Matrix2png: a utility for visualizing matrix data. *Bioinformatics* 19(2):295.
- Perez-Cerda C, Merinero B, Sanz P, Jimenez A, Garcia MJ, Urbon A, Diaz Recasens J, Ramos C, Ayuso C, Ugarte M. 1989. Successful first trimester diagnosis in a pregnancy at risk for propionic acidemia. *J Inherit Metab Dis* 12 Suppl 2:274-6.

- 1  
2  
3 Perez B, Desviat LR, Gomez-Puertas P, Martinez A, Stevens RC, Ugarte M. 2005.  
4  
5 Kinetic and stability analysis of PKU mutations identified in BH4-responsive  
6  
7 patients. *Mol Genet Metab* 86 Suppl 1:S11-6.  
8  
9  
10 Pey AL, Desviat LR, Gamez A, Ugarte M, Perez B. 2003. Phenylketonuria: Genotype-  
11  
12 phenotype correlations based on expression analysis of structural and functional  
13  
14 mutations in PAH. *Hum Mutat* 21(4):370-8.  
15  
16  
17 Pey AL, Perez B, Desviat LR, Martinez MA, Aguado C, Erlandsen H, Gamez A, Stevens  
18  
19 RC, Thorolfsson M, Ugarte M and others. 2004. Mechanisms underlying  
20  
21 responsiveness to tetrahydrobiopterin in mild phenylketonuria mutations. *Hum*  
22  
23 *Mutat* 24(5):388-99.  
24  
25  
26  
27 Pey AL, Stricher F, Serrano L, Martinez A. 2007. Predicted effects of missense  
28  
29 mutations on native-state stability account for phenotypic outcome in  
30  
31 phenylketonuria, a paradigm of misfolding diseases. *Am J Hum Genet*  
32  
33 81(5):1006-24.  
34  
35  
36  
37 Pey AL, Ying M, Cremades N, Velazquez-Campoy A, Scherer T, Thony B, Sancho J,  
38  
39 Martinez A. 2008. Identification of pharmacological chaperones as potential  
40  
41 therapeutic agents to treat phenylketonuria. *J Clin Invest* 118(8):2858-67.  
42  
43  
44 Rincon A, Aguado C, Desviat LR, Sanchez-Alcudia R, Ugarte M, Perez B. 2007.  
45  
46 Propionic and Methylmalonic Acidemia: Antisense Therapeutics for Intronic  
47  
48 Variations Causing Aberrantly Spliced Messenger RNA. *Am J Hum Genet*  
49  
50 81(6):1262-70.  
51  
52  
53 Saridakis V, Yakunin A, Xu X, Anandakumar P, Pennycooke M, Gu J, Cheung F, Lew  
54  
55 JM, Sanishvili R, Joachimiak A and others. 2004. The structural basis for  
56  
57  
58  
59  
60

1  
2  
3 methylmalonic aciduria. The crystal structure of archaeal ATP:cobalamin  
4  
5 adenosyltransferase. *J Biol Chem* 279(22):23646-53.  
6  
7

8 Schubert HL, Hill CP. 2006. Structure of ATP-Bound Human ATP:Cobalamin  
9  
10 Adenosyltransferase. *Biochemistry* 45(51):15188-96.  
11

12 St Maurice M, Mera PE, Taranto MP, Sesma F, Escalante-Semerena JC, Rayment I.  
13  
14 2007. Structural characterization of the active site of the PduO-type  
15  
16 ATP:Co(I)rrinoid adenosyltransferase from *Lactobacillus reuteri*. *J Biol Chem*  
17  
18 282(4):2596-605.  
19  
20  
21

22 Still WC, Tempczyk A, Hawley RC, Hendrickson T. 2002. Semianalytical treatment of  
23  
24 solvation for molecular mechanics and dynamics. *Journal of the American*  
25  
26 *Chemical Society* 112(16):6127-6129.  
27  
28

29 Weiser J, Shenkin PS, Still WC. 1999. Approximate atomic surfaces from linear  
30  
31 combinations of pairwise overlaps (LCPO). *Journal of Computational Chemistry*  
32  
33 20(2):217-230.  
34  
35

36 William LJ, Jayaraman C, Jeffry DM, Roger WI, Michael LK. 1983. Comparison of  
37  
38 simple potential functions for simulating liquid water. *The Journal of Chemical*  
39  
40 *Physics* 79(2):926-935.  
41  
42

43 Yamanishi M, Labunska T, Banerjee R. 2005. Mirror "base-off" conformation of  
44  
45 coenzyme B12 in human adenosyltransferase and its downstream target,  
46  
47 methylmalonyl-CoA mutase. *J Am Chem Soc* 127(2):526-7.  
48  
49

50 Zhang J, Dobson CM, Wu X, Lerner-Ellis J, Rosenblatt DS, Gravel RA. 2006. Impact of  
51  
52 cblB mutations on the function of ATP:cob(I)alamin adenosyltransferase in  
53  
54 disorders of vitamin B12 metabolism. *Mol Genet Metab* 87(4):315-22.  
55  
56  
57  
58  
59  
60

## FIGURE LEGENDS

**Figure 1.** Schematic representation of the mutations mapped in genomic DNA and RT-PCR pattern from fibroblast and minigenes assay. A) Patient P2 carries one nucleotide change located on exon 7 (c.584G>A) and a missense change on exon 3 (c.287C>T; p.I96T). The transcriptional profile shows three bands corresponding to the skipping of exon 7 transcribed from the allele bearing the c.584G>A change, a normal band from the allele bearing the c.287 T>C and a heteroduplex extra band (upper band). B) Patient 4 carries a change located on the last nucleotide of exon 3 (c.290 G>A) and an intronic change (c.349-1G>C) in intron 4. The RT-PCR pattern shows a smaller band without exon 3 resulting from the c.290G>A change and a larger one with an in-frame deletion of the first six nucleotides of exon 5 from the allele bearing c.349-1G>C.

**Figure 2.** Splicing cellular minigene analysis. RT-PCR pattern obtained after transfection with the corresponding wild-type and mutant minigene constructs and schematic representation of each minigene construct. The PCR from the c.290G>A and c.349-1G>A minigenes was performed using minigene-specific primers while in the c.584G>A, a specific forward primer located at the junction of the vector sequence and exon 6 was used to prevent different bands obtained when minigene-specific primers are used. All fragments were sequenced and the schematic representation of the resultant transcripts is indicated. Gene fragments corresponding to exon 3 (A) or exon 5 (B) and flanking 3' and 5' intronic regions were amplified from patients and cloned into the pSPL3 vector (grey line and box). For the c.584G>A minigene, the amplified fragment included exon 6, intron 6 and exon 7 and also the intronic sequence adjacent

1  
2  
3 to both exons. The exonic sequences of the pSPL3 vector are highlighted in black  
4 boxes (V-boxes: vector sequence) and striped boxes refers to the sequences involved  
5 when the cryptic splice sites are used (A and C). The sequence of the RT-PCR  
6 fragment obtained with the normal minigene (c.290G, c.349-1G and c.584G) revealed  
7 the presence of a normal transcript with the corresponding exon included. In the two  
8 former cases we have also detected a slight band corresponding to a complete skipping  
9 of exon 3 and 5 that cannot be amplified in the third case. The sequence of the  
10 fragment obtained after transfection with the mutant construction containing the c.290A  
11 or c.584A changes revealed the presence of a vector sequence of 119bp inserted in the  
12 aberrant transcript due to activation of a 3' and 5' cryptic splice site located in the vector  
13 sequence following the poly-cloning site.  
14  
15  
16  
17  
18  
19  
20  
21  
22  
23  
24  
25  
26  
27  
28  
29  
30  
31

**Figure 3.** Structural analysis of missense mutation. A) Location of the p.I96T and  
32 p.R191W mutations in the crystal structure of human ATR. The enzyme is a  
33 homotrimer, with each subunit (shown in a different shade of blue) composed of a five-  
34 helix bundle and with the active site located at the subunit interfaces. Residue I96 is  
35 located in helix  $\alpha$ 1, distant from the ATP binding site while residue R191 projects into  
36 the central cavity of the trimeric protein. ATP (red) and the residues, I96 (blue) and  
37 R191 (gold) are shown in stick representation. This figure was generated from the PDB  
38 file 2idx. B) Wild-type hATR trimer core (represented as cartoon) showing hydrogen  
39 bonds (dashed yellow lines) between residues E91, R190 and R191 (represented as  
40 sticks). C) R191W mutant hATR trimer core (represented as cartoons) showing  
41  
42  
43  
44  
45  
46  
47  
48  
49  
50  
51  
52  
53  
54  
55  
56  
57  
58  
59  
60

1  
2  
3 hydrogen bonds (dashed yellow lines) between residues E91, R190 and R191  
4  
5 (represented as sticks).  
6  
7  
8  
9

10 **Figure 4.** Oligomeric state of ATR. Blue native gel electrophoresis of cell extracts  
11 subjected to immunodetection for ATR. Lane 1, 1  $\mu\text{g}$  of purified wild-type hATR; lane 2,  
12 total extract from non-transformed BL21 bacteria; lanes 3-5, whole cell extracts from  
13 uninduced bacteria transformed with wild-type ATR plasmid (lane 3), p.I96T ATR (lane  
14 4) and p.R191W ATR (lane 5); Lanes 6-14 induced transformed bacteria. Lanes 6, 7  
15 and 8, whole cell extracts of wild-type (1  $\mu\text{g}$ ), p.I96T (2.5  $\mu\text{g}$ ) or p.R191W (20  $\mu\text{g}$ ); lanes  
16 9, 10 and 11, supernatant of wild-type (1  $\mu\text{g}$ ), p.I96T (2.5  $\mu\text{g}$ ) and p.R191W (20  $\mu\text{g}$ )  
17 after centrifugation of sonicated cell extracts; lanes 12, 13 and 14, pellets from wild-type  
18 (1  $\mu\text{g}$ ), p.I96T (2.5  $\mu\text{g}$ ) and p.R191W (20  $\mu\text{g}$ ) obtained after centrifugation.  
19  
20  
21  
22  
23  
24  
25  
26  
27  
28  
29  
30  
31  
32  
33

34 **Figure 5.** Degradation time course for wild-type p.I96T and p.R191W ATR at 37°C and  
35 27°C. Crude cell extracts from cultures expressing wild-type or p.I96T or p.R191W ATR  
36 were incubated at 37°C (A) or 27°C (B) and aliquots were removed at different time  
37 points at 37 and 27°C respectively and subjected to SDS-PAGE and Western blot  
38 analysis as described in methods. Protein amounts were quantified by laser  
39 densitometry. The data are the mean  $\pm$  SD and represent the percent density of each  
40 protein relative to its density at time 0. The half-life of each protein is noted.  
41  
42  
43  
44  
45  
46  
47  
48  
49  
50  
51  
52

53 **Figure 6.** Functional analysis of the p.I96T and p.R191W mutants in a *cbIB* null  
54 fibroblast cell line. A fibroblast cell line was transfected with a vector encoding wild-type  
55  
56  
57  
58  
59  
60

1  
2  
3 or mutant (p.I96T or p.R191W) *MMAB* cDNA and the culture was incubated at 37 or  
4  
5 27°C. The cells were harvested followed by incorporation of [<sup>14</sup>C]-propionate into  
6  
7 trichloroacetic acid-precipitable material in the absence of OHCbl that was quantified as  
8  
9 an indirect measure of ATR activity. The data are the mean ± SD of the percentage of  
10  
11 [<sup>14</sup>C]-propionate incorporation for each transfection versus the wild-type transfection  
12  
13 (n=4). The p-values were calculated for the pairs indicated in the figure (\*\*\*) = p-value  
14  
15 <0.001).  
16  
17  
18  
19  
20  
21  
22  
23  
24  
25  
26  
27  
28  
29  
30  
31  
32  
33  
34  
35  
36  
37  
38  
39  
40  
41  
42  
43  
44  
45  
46  
47  
48  
49  
50  
51  
52  
53  
54  
55  
56  
57  
58  
59  
60

For Peer Review

**Table 1. Genotype, clinical and biochemical phenotype in four methylmalonic aciduria patients *cbIB* type**

Patient	MUT activity** (nmol/min/mg)	[1- <sup>14</sup> C]-propionate -/+ ***	Allele 1	Allele 2	Onset	Outcome
P1	0.99	0.06/0.25	p.I96T (c.287T>C)	p.R191W (c.571C>T)	Neonatal (4 days)	7y/ severe encephalopathy
P2*	0.76	0.26/1.01	p.I96T (c.287T>C)	p.S174fs (c.584G>A)	Late onset (4 years)	Died at 4y
P3*	NS	NS	p.I96T (c.287T>C)	p.S174fs (c.584G>A)	studied due to previous affected sister (3 months)	5y/ asymptomatic
P4	0.55	0.08/0.07	p.I117_Q118del (c.349-1G>C)	p.G66fs (c.290G>A)	Neonatal (4 days)	12y/ asymptomatic

\* Patients 2 (P2) and 3 (P3) are siblings

\*\*MUT activity in control fibroblasts with 36μM AdoCbl was 0.94±0.40 nmol/min/mg protein

\*\*\*[1-<sup>14</sup>C]-Propionate uptake (nmol/10h/mg protein) in control fibroblasts without/with (-/+) hydroxocobalamin in the culture medium was 1.90±1.18/2.34±1.61.

NS: not studied.

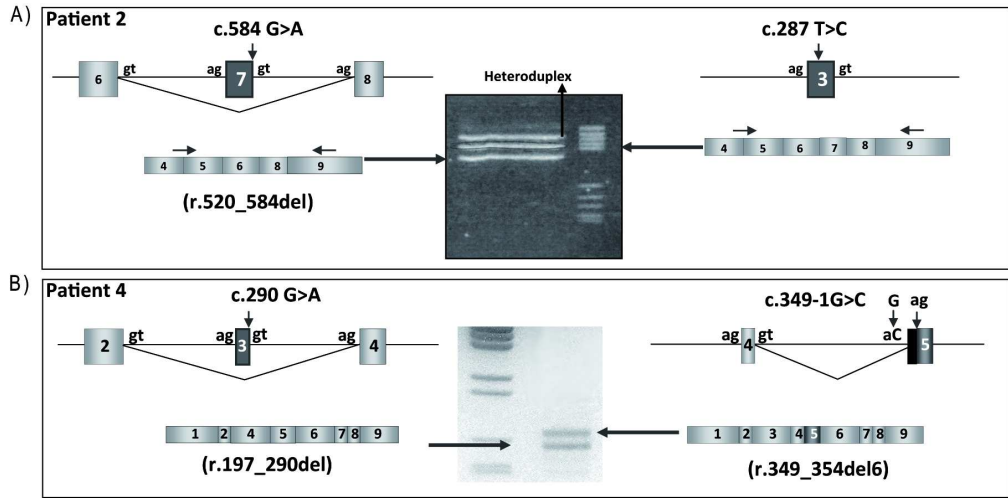
Mutation nomenclature follows the recommendations of HGVS and cDNA numbering is based on GenBank accession number NM\_052845.3

**Table 2. Comparison of kinetic parameters for wild-type and p.I96T ATR**

	wild-type	p.I96T
Specific activity (nmol min <sup>-1</sup> mg <sup>-1</sup> )	200 ± 10	123 ± 19
K <sub>M</sub> (μM) ATP	6.2 ± 1.3	7.8 ± 1.9
K <sub>d</sub> (μM) AdoCbl	1.7 ± 0.4	2.58 ± 0.62
K <sub>d</sub> (μM) OHCbl	8.5 ± 1.1	7.8 ± 1.6
K <sub>d</sub> (μM) CNCbl	7.8 ± 0.5	13.3 ± 0.3
K <sub>d</sub> (μM) Cob(II)alamin	3.6 ± 1.6	1.37 ± 0.33

Data are the mean of at least two independent experiments each performed in duplicate

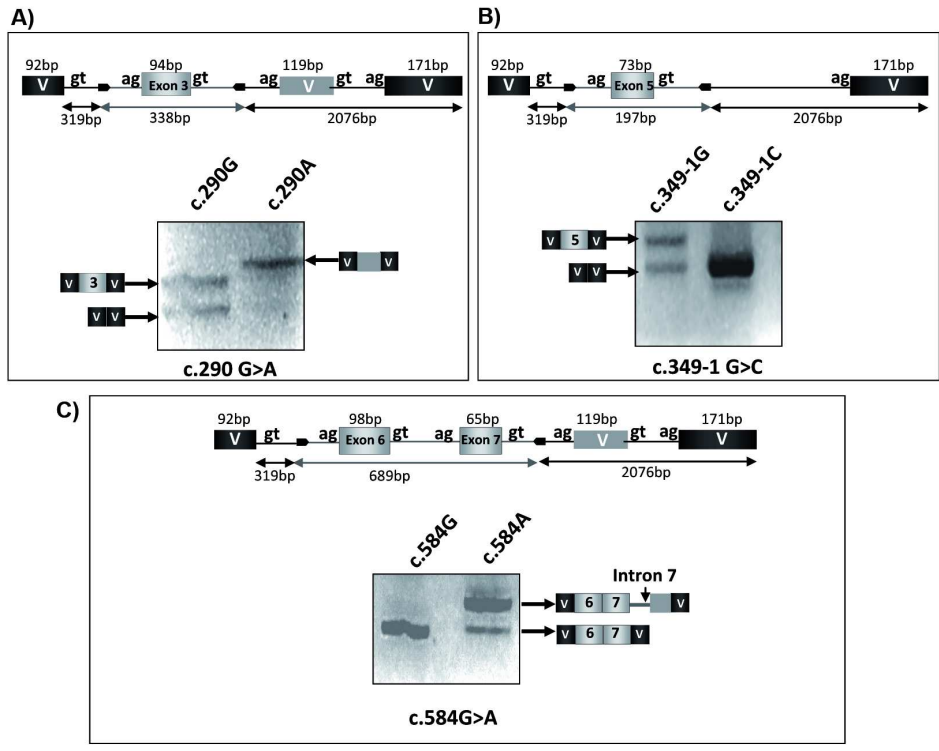
1  
2  
3  
4  
5  
6  
7  
8  
9  
10  
11  
12  
13  
14  
15  
16  
17  
18  
19  
20  
21  
22  
23  
24  
25  
26  
27  
28  
29  
30  
31  
32  
33  
34  
35  
36  
37  
38  
39  
40  
41  
42  
43  
44  
45  
46  
47  
48  
49  
50  
51  
52  
53  
54  
55  
56  
57  
58  
59  
60



229x113mm (200 x 200 DPI)

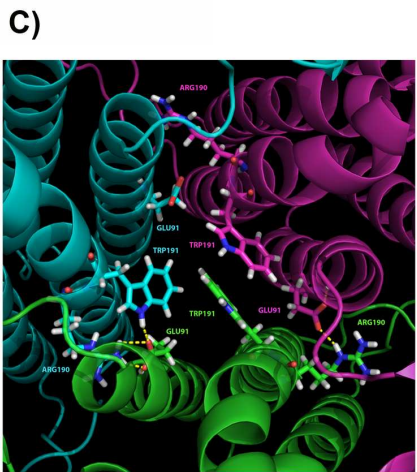
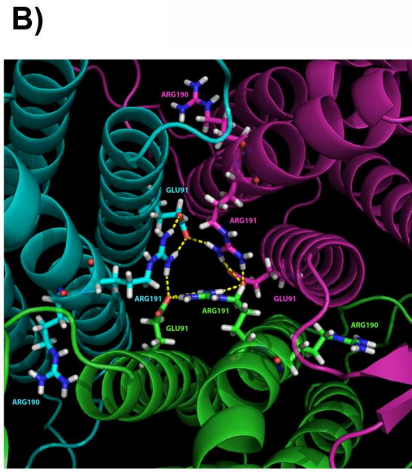
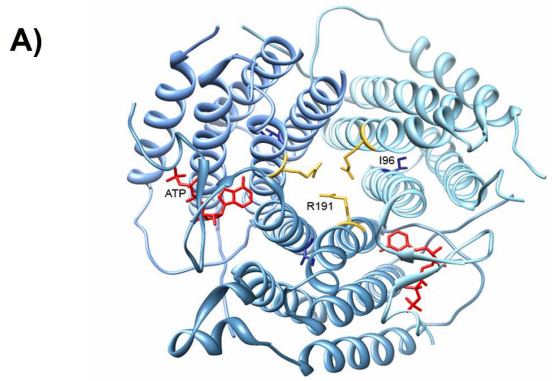
Peer Review

1  
2  
3  
4  
5  
6  
7  
8  
9  
10  
11  
12  
13  
14  
15  
16  
17  
18  
19  
20  
21  
22  
23  
24  
25  
26  
27  
28  
29  
30  
31  
32  
33  
34  
35  
36  
37  
38  
39  
40  
41  
42  
43  
44  
45  
46  
47  
48  
49  
50  
51  
52  
53  
54  
55  
56  
57  
58  
59  
60



219x170mm (200 x 200 DPI)

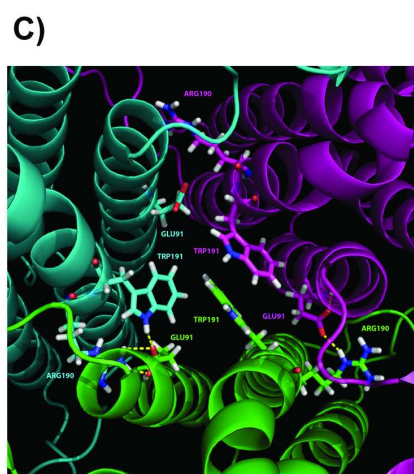
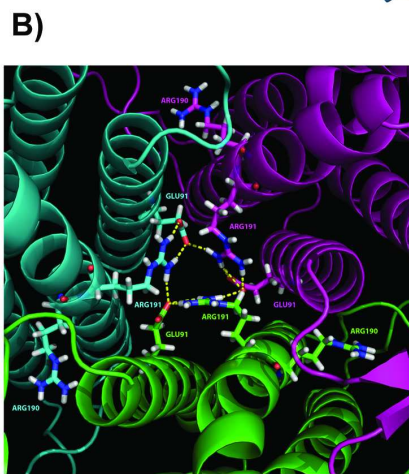
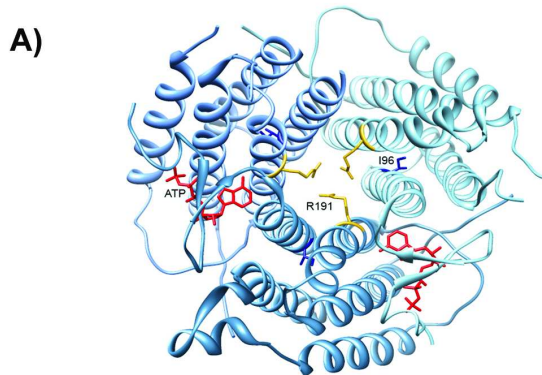
1  
2  
3  
4  
5  
6  
7  
8  
9  
10  
11  
12  
13  
14  
15  
16  
17  
18  
19  
20  
21  
22  
23  
24  
25  
26  
27  
28  
29  
30  
31  
32  
33  
34  
35  
36  
37  
38  
39  
40  
41  
42  
43  
44  
45  
46  
47  
48  
49  
50  
51  
52  
53  
54  
55  
56  
57  
58  
59  
60



150x143mm (300 x 300 DPI)

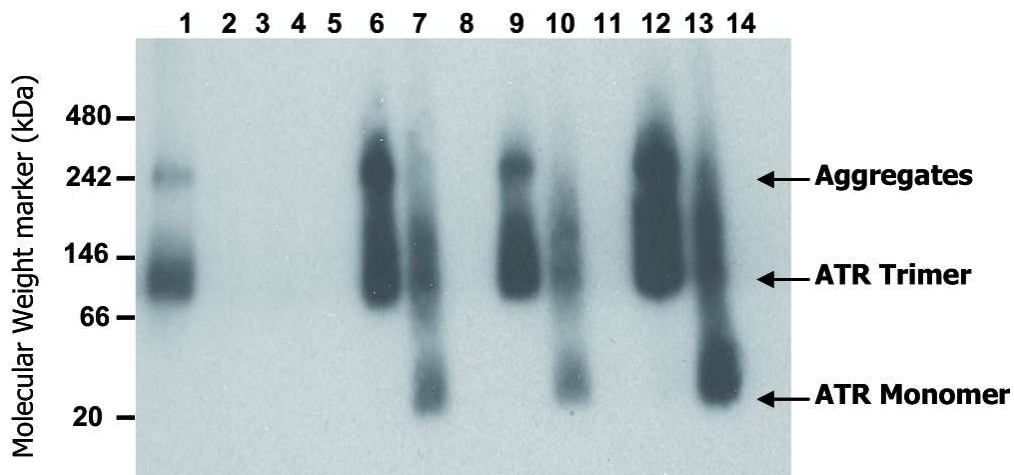


1  
2  
3  
4  
5  
6  
7  
8  
9  
10  
11  
12  
13  
14  
15  
16  
17  
18  
19  
20  
21  
22  
23  
24  
25  
26  
27  
28  
29  
30  
31  
32  
33  
34  
35  
36  
37  
38  
39  
40  
41  
42  
43  
44  
45  
46  
47  
48  
49  
50  
51  
52  
53  
54  
55  
56  
57  
58  
59  
60



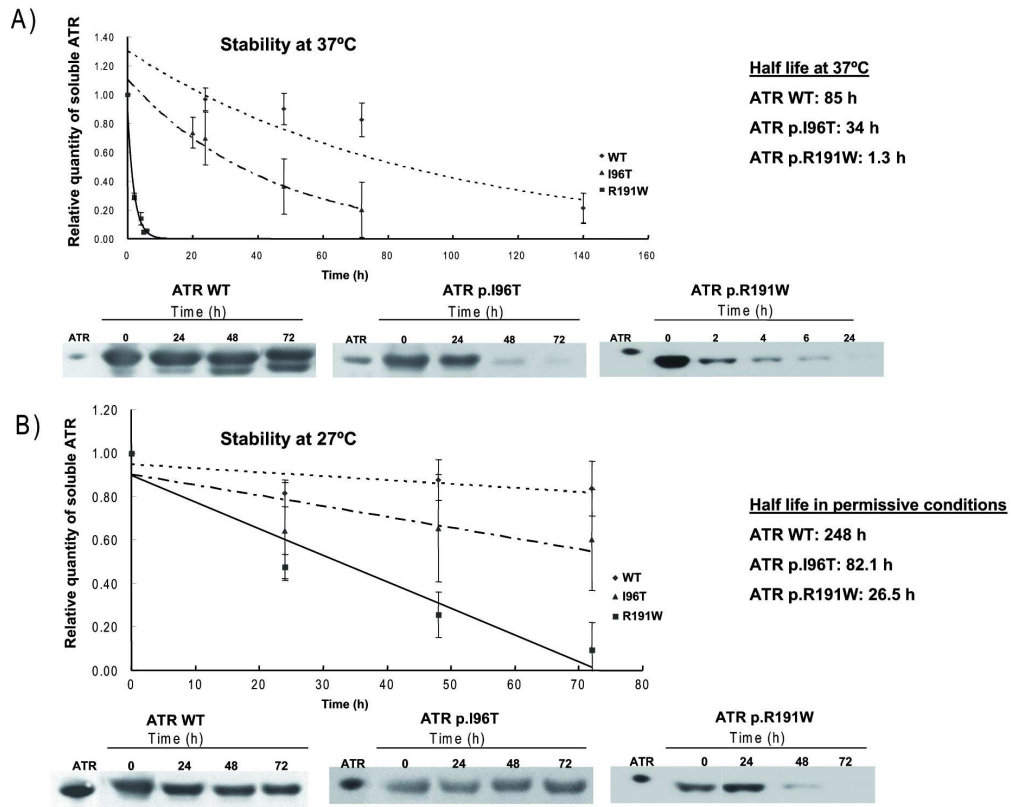
150x143mm (300 x 300 DPI)





127x59mm (200 x 200 DPI)

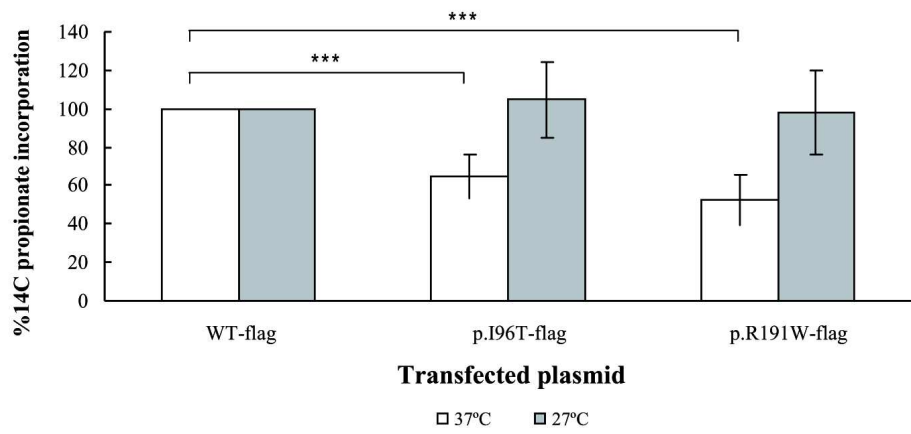
Peer Review



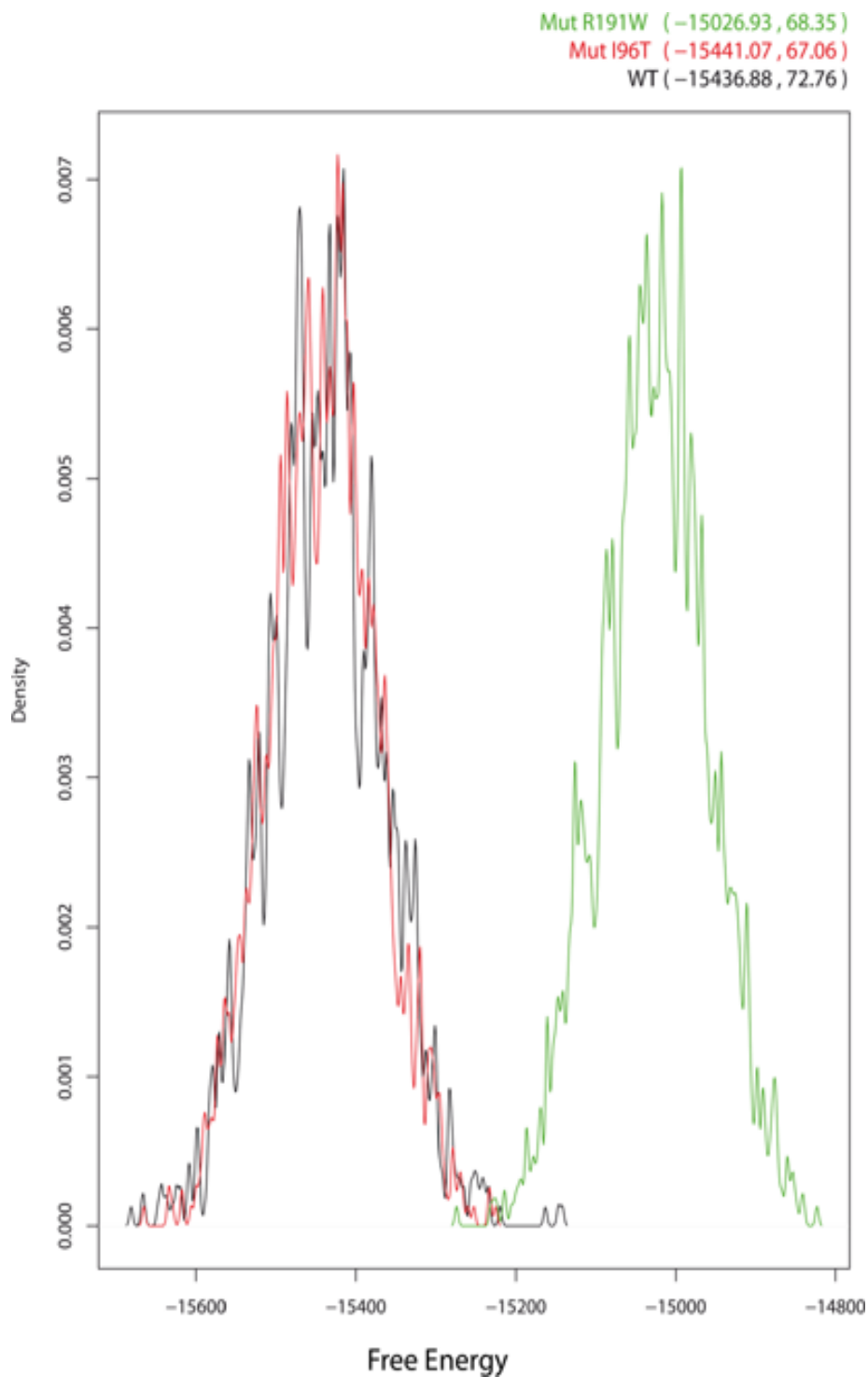
234x188mm (200 x 200 DPI)

view

1  
2  
3  
4  
5  
6  
7  
8  
9  
10  
11  
12  
13  
14  
15  
16  
17  
18  
19  
20  
21  
22  
23  
24  
25  
26  
27  
28  
29  
30  
31  
32  
33  
34  
35  
36  
37  
38  
39  
40  
41  
42  
43  
44  
45  
46  
47  
48  
49  
50  
51  
52  
53  
54  
55  
56  
57  
58  
59  
60



189x117mm (200 x 200 DPI)



**Supp. Figure S1.** Density distribution of the observed free energies in wild-type hATR (black), mutant p.I96T (red) and mutant p.R191W (green) ATR proteins.